

Robert B. Clark, Matteo E. Mangoni, Andreas Lueger, Brigitte Couette, Joel Nargeot and Wayne R. Giles

Am J Physiol Heart Circ Physiol 286:1757-1766, 2004. First published Dec 23, 2003;
doi:10.1152/ajpheart.00753.2003

You might find this additional information useful...

This article cites 42 articles, 33 of which you can access free at:

<http://ajpheart.physiology.org/cgi/content/full/286/5/H1757#BIBL>

This article has been cited by 5 other HighWire hosted articles:

Ether-a-go-go-related gene 3 is the main candidate for the E-4031-sensitive potassium current in the pacemaker interstitial cells of Cajal

E. J. White, S. J. Park, J. A. Foster and J. D. Huizinga

Am J Physiol Gastrointest Liver Physiol, October 1, 2008; 295 (4): G691-G699.

[Abstract] [Full Text] [PDF]

Genesis and Regulation of the Heart Automaticity

M. E. Mangoni and J. Nargeot

Physiol Rev, July 1, 2008; 88 (3): 919-982.

[Abstract] [Full Text] [PDF]

Erg K⁺ channels modulate contractile activity in the bovine epididymal duct

M. Mewe, I. Wulfsen, A. M. E. Schuster, R. Middendorff, G. Glassmeier, J. R. Schwarz and C. K. Bauer

Am J Physiol Regulatory Integrative Comp Physiol, March 1, 2008; 294 (3): R895-R904.

[Abstract] [Full Text] [PDF]

Molecular Physiology of Cardiac Repolarization

J. M. Nerbonne and R. S. Kass

Physiol Rev, October 1, 2005; 85 (4): 1205-1253.

[Abstract] [Full Text] [PDF]

Heterogeneity of action potential durations in isolated mouse left and right atria recorded using voltage-sensitive dye mapping

A. Nygren, A. E. Lomax and W. R. Giles

Am J Physiol Heart Circ Physiol, December 1, 2004; 287 (6): H2634-H2643.

[Abstract] [Full Text] [PDF]

Updated information and services including high-resolution figures, can be found at:

<http://ajpheart.physiology.org/cgi/content/full/286/5/H1757>

Additional material and information about *AJP - Heart and Circulatory Physiology* can be found at:

<http://www.the-aps.org/publications/ajpheart>

This information is current as of July 11, 2009 .

A rapidly activating delayed rectifier K^+ current regulates pacemaker activity in adult mouse sinoatrial node cells

Robert B. Clark,¹ Matteo E. Mangoni,² Andreas Lueger,³
Brigitte Couette,² Joel Nargeot,² and Wayne R. Giles¹

¹Department of Physiology and Biophysics, University of Calgary Health Sciences Centre, Calgary, Alberta, Canada T2N 4N1; ²Laboratoire de Genomique Fonctionnelle, Centre National de la Recherche Scientifique UPR 2580, and Institut de Genetique Humaine, Centre National de la Recherche Scientifique UPR 1142, 34396 Montpellier Cedex 5, France; and ³Department of Internal Medicine, Karl-Franzens-University Hospital, 8036 Graz, Austria

Submitted 6 August 2003; accepted in final form 17 December 2003

Clark, Robert B., Matteo E. Mangoni, Andreas Lueger, Brigitte Couette, Joel Nargeot, and Wayne R. Giles. A rapidly activating delayed rectifier K^+ current regulates pacemaker activity in adult mouse sinoatrial node cells. *Am J Physiol Heart Circ Physiol* 286: H1757–H1766, 2004. First published December 23, 2003; 10.1152/ajpheart.00753.2003.—We have investigated the physiological role of the “rapidly activating” delayed rectifier K^+ current (I_{Kr}) in pacemaker activity in isolated sinoatrial node (SAN) myocytes and the expression of mouse *ether-a-go-go* (mERG) genes in the adult mouse SAN. In isolated, voltage-clamped SAN cells, outward currents evoked by depolarizing steps (greater than -40 mV) were strongly inhibited by the class III methanesulfonanilide compound E-4031 (1 – 2.5 μ M), and the deactivation “tail” currents that occurred during repolarization to a membrane potential of -45 mV were completely blocked. E-4031-sensitive currents (I_{Kr}) reached a maximum at a membrane potential of -10 mV and showed pronounced inward rectification at more-positive membrane potentials. Activation of I_{Kr} occurred at -40 to 0 mV, with half-activation at about -24 mV. The contribution of I_{Kr} to action potential repolarization and diastolic depolarization was estimated by determining the E-4031-sensitive current evoked during voltage clamp with a simulated mouse SAN action potential. I_{Kr} reached its peak value (~ 0.6 pA/pF) near -25 mV, close to the midpoint of the repolarization phase of the simulated action potential, and deactivated almost completely during the diastolic interval. E-4031 (1 μ M) slowed the spontaneous pacing rate of Langendorff-perfused, isolated adult mouse hearts by an average of 36.5% ($n = 5$). Expression of mRNA corresponding to three isoforms coded by the mouse ERG1 gene (mERG1, mERG1a, mERG1a', and mERG1b), was consistently found in the SAN. Our data provide the first detailed characterization of I_{Kr} in adult mouse SAN cells, demonstrate that this current plays an important role in pacemaker activity, and indicate that multiple isoforms of mERG1 can contribute to native SAN I_{Kr} .

sinus node; E-4031; mERG1

THE “RAPIDLY ACTIVATING” DELAYED rectifier K^+ current (I_{Kr}) has an important role in repolarization of cardiac myocytes in many mammalian species, including humans. Indeed, mutations in the human *ether-a-go-go* (ERG) gene (HERG1), which codes for the cardiac I_{Kr} , lead to the long-QT syndrome and increase the susceptibility to drug-induced arrhythmias (13, 27).

I_{Kr} was first described in guinea pig ventricular (28) and atrial (29) cells, and the properties of I_{Kr} have subsequently

been characterized in a wide variety of other mammalian cardiac myocytes (34). In addition to its role in action potential repolarization in atrial and ventricular myocytes, I_{Kr} has also been shown to contribute to repolarization and pacemaking in the sinoatrial node (SAN) of mammalian heart (4, 11, 35). Class III antiarrhythmic methanesulfonanilide drugs such as dofetilide (UK-68798) and E-4031, at concentrations that block I_{Kr} selectively, reduce the spontaneous pacing rate, slow the rate of repolarization, and depolarize the maximum diastolic potential of single pacemaking cells isolated from rabbit (14, 18, 24, 25) and guinea pig (22) SAN.

I_{Kr} has been identified in mouse fetal (7, 38, 39) and neonatal (23, 24, 39) ventricular myocytes and, at a much lower level of expression, in the ventricle of adult mice (3) and rats (25, 40). On the basis of the effect of dofetilide on action potential duration, I_{Kr} plays an important role in action potential repolarization in ventricular myocytes of fetal and neonatal mouse heart; most of the outward current in voltage-clamped fetal ventricular myocytes was blocked by dofetilide (38, 39). On the other hand, the role of I_{Kr} in repolarization in adult mouse and rat myocytes remains unclear. For example, dofetilide had no measurable effect on the action potential duration of adult mouse ventricular myocytes (39) or rat papillary muscles and atria (33). In adult rat atrial (25) and ventricular (25, 40) myocytes, the E-4031-sensitive currents were very small compared with the other repolarizing K^+ currents in these cell types (2, 5).

The role of I_{Kr} in repolarization and pacemaking in adult mouse SAN has not previously been examined. Evidence for the presence of I_{Kr} in mouse SAN cells was presented recently (6, 21), but no detailed information on its physiological role is available. The present study characterizes the properties of I_{Kr} in adult mouse SAN cells and demonstrates that this K^+ current has an important role in action potential repolarization and pacemaking. Furthermore, we show that mouse SAN expresses multiple isoforms of mouse ERG1 (mERG1), which thus constitutes the molecular basis of native “pacemaker” I_{Kr} in mouse SAN cells. Our results will help in the development of genetically modified mouse strains designed to dissect the functional role of mERG channels in cardiac pacemaker activity.

Address for reprint requests and other correspondence: R. B. Clark, Dept. of Physiology and Biophysics, Health Sciences Centre, Univ. of Calgary, 3330 Hospital Dr., NW, Calgary, AB, Canada T2N 4N1 (E-mail: rclar@ucalgary.ca).

The costs of publication of this article were defrayed in part by the payment of page charges. The article must therefore be hereby marked “advertisement” in accordance with 18 U.S.C. Section 1734 solely to indicate this fact.

METHODS

All experiments followed the guidelines of the Canadian Council on Animal Care and were approved by the University of Calgary Health Sciences Animal Welfare Committee.

Isolation of single mouse SAN cells. Single cells were isolated from SAN of adult C57BL/6J mice of either gender (20–30 g body wt, 3–6 mo old) using the method described in detail previously (21).

Electrophysiological recordings from single SAN cells. Aliquots (~200–300 μ l) of cell suspension were plated into six to eight recording dishes that were stored in a refrigerator at $\sim 4^{\circ}\text{C}$ for 30–60 min to allow the cells to settle to the bottom of the dishes. A dish was placed on a heated stage of an inverted microscope (Nikon Diaphot) and continuously superfused with normal HEPES-buffered Tyrode solution containing (in mM) 140 NaCl, 5.4 KCl, 1.8 CaCl_2 , 1 MgCl_2 , 5 HEPES, and 5.5 D-glucose, with pH adjusted to 7.4 with NaOH. The temperature of the superfusion solution was maintained at 28 ± 1 or $35 \pm 1^{\circ}\text{C}$.

Membrane currents and action potentials were recorded in whole cell patch-clamp mode (27) using a MultiClamp 700A amplifier (Axon Instruments, Union City, CA). Currents and voltages were digitized and voltage-clamp protocols were generated with a Digidata 1322A data-acquisition interface controlled with pClamp 8 software (Axon Instruments). Patch pipettes were filled with a solution containing (in mM) 135 KCl, 1 MgCl_2 , 4 Mg-ATP, 0.1 Na-GTP, 5 EGTA, 5 HEPES, and 6.6 Na-phosphocreatine, with pH adjusted to 7.2 with KOH and direct-current resistance in the range 4–9 M Ω .

Action potentials were recorded using the amphotericin-perforated patch method (26). The patch pipette solution contained amphotericin (200 $\mu\text{g}/\text{ml}$). Action potentials were recorded in the presence of 10 nM isoproterenol (Iso). Although cells paced in the absence of Iso, the pacing rate of cells in the presence of this small concentration of Iso was much more stable for the 10–15 min required for experiments involving addition and removal of E-4031 (see Fig. 4).

Langendorff-perfused mouse hearts. Adult male C57BL/6J mice were treated with 200 U of heparin and killed 15 min later by cervical dislocation. The heart was rapidly excised and placed in ice-cold Krebs-Henseleit buffer. The aorta was cannulated for Langendorff perfusion with a vertically mounted 21-gauge stainless steel tube, and the heart was then retrogradely perfused via a water-jacketed heating coil at ~ 2 ml/min with warmed Krebs-Henseleit solution. The heart was immersed in Krebs-Henseleit solution in a warmed water-jacketed Lucite chamber. The entire perfusion apparatus was enclosed in an insulated environmental chamber with a volume of ~ 0.3 m³ in which the inside temperature was maintained at 37°C with an air temperature controller (Air-Therm, W. P. Instruments, Sarasota, FL). The temperature of the heart, monitored with a thermocouple temperature probe, was maintained at $37.2 \pm 0.2^{\circ}\text{C}$.

A pair of Ag-AgCl electrodes connected to a low-noise differential amplifier was placed on the left ventricle to record an ECG. Heart rate was analyzed online with custom software (Cardiolyzer, Laback, Graz, Austria) and stored in a microcomputer for later analysis.

The Krebs-Henseleit buffer contained (in mM) 118.5 NaCl, 25 NaHCO_3 , 4.7 KCl, 1.2 MgSO_4 , 1.2 KH_2PO_4 , 1.0 CaCl_2 , and 11 glucose, with pH adjusted to 7.4 after bubbling with a gas mixture of 95% O_2 -5% CO_2 at 37°C .

RT-PCR. Tissue samples used for mRNA purification were isolated from eight C57BL/6J male mice (4 mo of age, 20–23 g body wt). For RT-PCR analysis, total RNAs from the SAN, the right atrium, and the left ventricle were extracted using the SNAP kit (Invitrogen, Carlsbad, CA). RT-PCR was performed with total RNA using oligo(dT)_{12–18} primers and Superscript II RNase H reverse transcriptase (Invitrogen). After reverse transcription, the cDNAs for mERG1a, mERG1a', mERG1b, mERG2, and mERG3 were amplified using the following set of primers (from 5' to 3'): ACA CCT TCC TCG ACA CCA TC (sense; position 621–641, accession no. AF012870) and GCA TCA GGG TTA AGG CTC TG (antisense; position 1405–1424, accession

no. AF012871) for mERG1a, ACC ACT GGC ATA GGA CCA AG (sense; position 839–858, accession no. AF012870) and the same antisense as for mERG1a for mERG1a', ATG GCG ATT CCA GCC GGG AA (sense; position 3952–3971, accession no. AF012871) and GAT GCC ATT GGT GTA GGA CC (antisense; position 8239–8258, accession no. AF012871) for mERG1b, TCG CTA CCA CAC TCA GAT GC (sense; position 68–87, accession no. AK038513) and TGC GTG GTC TTG AAC TTG AC (antisense; position 321–340, same accession no. as for sense) for mERG2, and CGG AAA CTT TTT GGG TTC AA (sense; position 480–499, accession no. AJ291608) and CTG CAG CAT GTC AGG GTA GA (antisense; position 738–757, same accession no. as for sense) for mERG3. PCR was performed in a final volume of 25 μ l containing 2 μ l of reverse transcription reaction, 10 pmol of each primer, 2.5 mM each dNTP (Pharmacia), 1.5 mM MgCl_2 , 5% DMSO, and 1 U of *Taq* polymerase (Invitrogen) in a thermal cycler (MJ Research, Waltham, MA) with the following cycling protocol: after 3 min at 94°C , 35 cycles (94°C , 45 s; annealing temperature, 45 s; 72°C , elongation time) of PCR were performed followed by a final elongation period of 10 min at 72°C . Annealing temperatures and elongation time were as follows: 57°C and 70 s for mERG1a and mERG1a', 56°C and 120 s for mERG1b, and 56°C and 30 s for mERG2 and mERG3. To investigate the presence and size of the amplified fragments, PCR products were identified in an ethidium bromide-stained agarose gel (1.5%) by electrophoresis. The predicted sizes of the PCR-generated fragments were 747 bp (mERG1a), 755 bp (mERG1a'), 1,109 bp (mERG1b), 273 bp (mERG2), and 277 bp (mERG3).

Chemicals and drugs. Chemicals used for all solutions were obtained from Sigma Chemical (St. Louis, MO). E-4031 was obtained from Wako Pure Chemicals Industries (Osaka, Japan).

Data analysis and statistics. ClampFit 8 software (Axon Instruments) was used to measure current-voltage (*I-V*) relations and to fit exponential functions to currents. Best-fit Boltzmann functions were determined, and data were plotted with Sigmaplot (SPSS Science, Chicago, IL). Action potential parameters were analyzed with IDL software (Research Systems, Boulder, CO). Statistical analysis was performed with Prism 3 or InStat (GraphPad Software, San Diego, CA). Values are means \pm SE.

RESULTS

The spontaneously active myocytes chosen for study had “spindle” or “elongated-spindle” morphology, as described previously (21). The mean capacitance of 50 such cells from 14 different cell preparations was 28.8 ± 1.3 pf.

E-4031-sensitive current in mouse SAN cells. Figure 1A illustrates the effect of the methanesulfonanilide compound E-4031 (2.5 μM), a specific blocker of I_{Kr} (28, 29), on a family of outward currents from one voltage-clamped pacemaker cell. The magnitude of the outward current was reduced by E-4031 at all membrane potentials, but this reduction was most evident at potentials in the range -30 to 0 mV, where slowly activating outward currents recorded in the absence of E-4031 were abolished, leaving smaller outward currents that activated much more rapidly at each potential. Currents at more-positive potentials (>0 mV) were also reduced in magnitude by E-4031, but the fractional reduction in total current magnitude was much smaller than at less-depolarized potentials (-30 to 0 mV). Figure 1A also shows that the slowly decaying tail currents that followed the depolarizing steps were completely abolished by E-4031.

Figure 1B compares mean *I-V* relations for a number of different cells before and after exposure to 1.5–2.5 μM E-4031. The control *I-V* relation was distinctly nonlinear, with a steep increase in magnitude between about -40 and 0 mV and a “plateau” between 0 and about $+20$ mV. In contrast, the

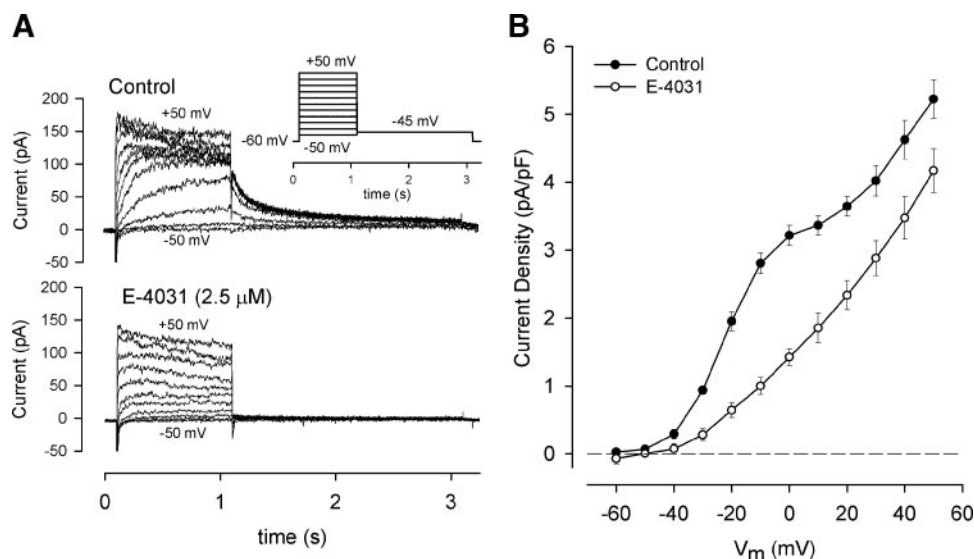


Fig. 1. A: family of membrane currents from a voltage-clamped, isolated mouse SAN cell (top). Inset: voltage-clamp protocol. Holding potential was -60 mV. Cell was stepped for 1 s to potentials between -50 and $+50$ mV in 10-mV increments. Each step was followed by a 2-s step to -45 mV and then to the holding potential. Cell capacitance was 33.3 pF. The same series of voltage-clamp steps was applied to the cell after 3 min of exposure to 2.5 μ M E-4031 (bottom). B: mean isochronal current-voltage (I - V) relations for current at the end of 1-s depolarizing steps in control cells ($n = 12$) and in the presence of 1.7–2.5 μ M E-4031 ($n = 9$). Currents from each cell were normalized to capacitance before averaging. Temperature was $28 \pm 1^\circ\text{C}$. V_m , membrane potential.

I - V relation after application of E-4031 increased uniformly from -40 mV to the maximum potential tested.

Figure 2A shows the family of E-4031-sensitive difference currents (I_{Kr}) obtained from the pacemaker myocyte shown in Fig. 1. In this cell, the threshold for activation of outward current was between -40 and -30 mV. The rate of activation of the current increased significantly with membrane depolarization. The largest outward current was recorded at a membrane potential of 0 mV, and the peak outward current then decreased significantly as the depolarization was increased beyond 0 mV. The slowly decaying tail current (deactivation of I_{Kr}) after the depolarizing steps increased in magnitude for steps up to about -10 mV and was approximately constant in magnitude for more-positive steps. The mean I - V relation for I_{Kr} for nine different cells is shown in Fig. 2B; note the region of “negative slope” for membrane potentials more positive than about -10 mV.

The membrane potential dependence of activation of I_{Kr} was determined from the amplitude of tail currents at -45 mV after the depolarizing steps. The amplitude of the tail current was estimated by fitting decaying exponential functions to the tail currents and extrapolating the fitted function back to the end of the depolarizing step (Fig. 2B). This procedure was used to correct the tail current amplitude for inactivation of I_{Kr} that occurred during the depolarizing step (32). Figure 2C is a plot of I_{Kr} tail current amplitude as a function of depolarization for 16 different cells. The data were fitted to a single Boltzmann function (Fig. 2C) in which half-activation of I_{Kr} occurred at about -24 mV.

Membrane potential dependence of I_{Kr} deactivation and activation kinetics. Figure 3A shows examples of I_{Kr} tail currents recorded at a series of different membrane potentials from -35 to -65 mV (within the range of the normal diastolic

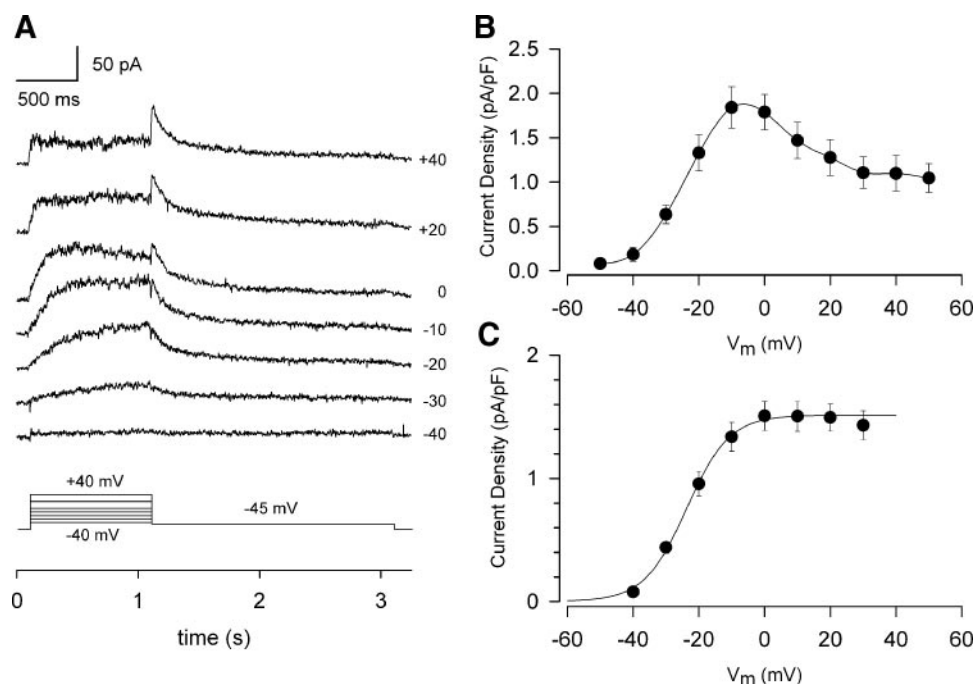


Fig. 2. A: family of E-4031-sensitive currents, I_{Kr} , from cell shown in Fig. 1 (top). Membrane potentials during 1-s depolarizing step are shown at right. Bottom: voltage-clamp protocol. B: I - V relation for isochronal I_{Kr} at the end of 1-s depolarizing steps. Currents from each cell were normalized to capacitance before averaging. Values are means \pm SE ($n = 9$). C: membrane potential dependence of I_{Kr} tail current amplitude. Tail current amplitude (at -45 mV) was determined from best-fit 2-exponential function of the following form: $I(t) = A \exp(-t/\tau_1) + B \exp(-t/\tau_2) + C$, where A and B are amplitude factors, τ_1 and τ_2 are time constants, and C is a time-independent baseline. Currents were normalized to cell capacitance and then averaged ($n = 16$). Solid line, best-fit single Boltzmann function: $I(V_m) = I_{max}/\{1 + \exp[-(V_m - V_h)/S_h]\}$, where I_{max} is maximum tail current amplitude (1.51 pA/pF), V_h is membrane potential for half-maximal activation (-23.7 mV), and S_h is a slope factor at V_h (6.5 mV). Temperature was $28 \pm 1^\circ\text{C}$.

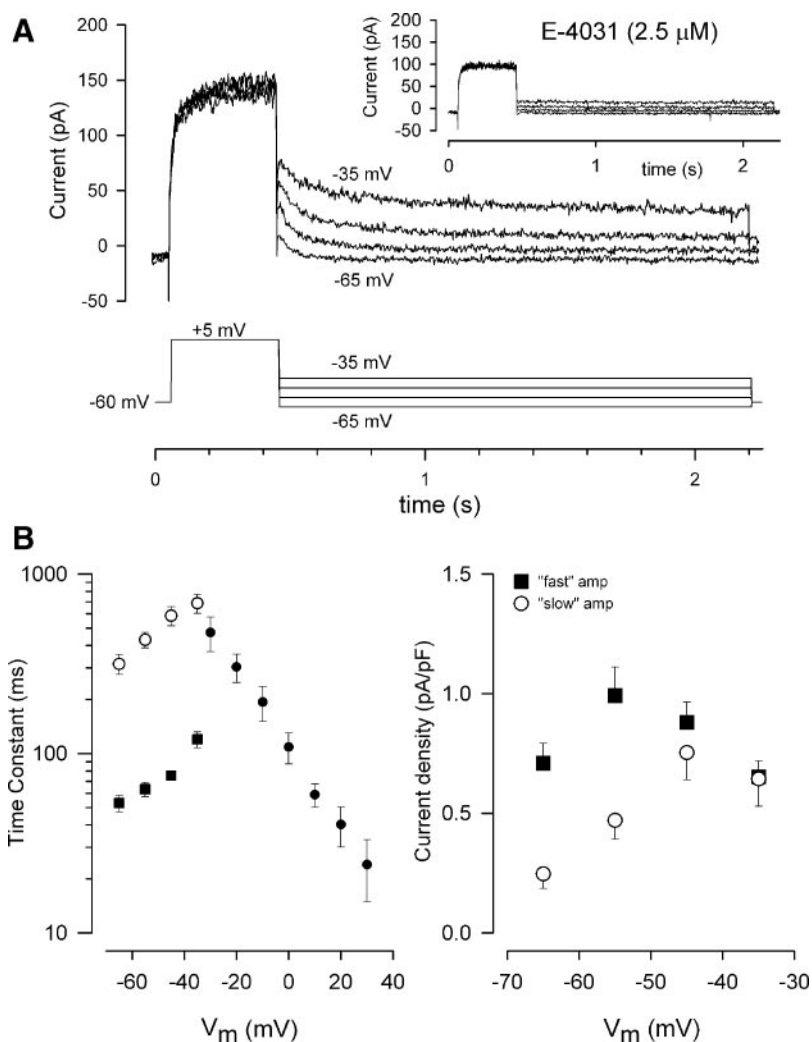


Fig. 3. A: family of deactivating I_{Kr} tail currents at selected membrane potentials between -35 and -65 mV. Voltage-clamp protocol is shown below current traces. *Inset*: currents in the presence of $2.5 \mu\text{M}$ E-4031. B: time constants of activation of I_{Kr} (●; means \pm SE, $n = 9$) and deactivation tail currents (○ and ■; means \pm SE, $n = 14$) as a function of membrane potential (*left*). Time constants were determined from single-exponential functions fitted to the onset of I_{Kr} and 2-exponential functions fitted to tail currents (see Fig. 2 legend). *Right*: amplitude of “fast” and “slow” components of 2-exponential functions fitted to tail currents vs. membrane potential. Values are means \pm SE ($n = 14$). Amplitudes were normalized to capacitance for each cell and then averaged. Temperature was $28 \pm 1^\circ\text{C}$.

depolarization or pacemaker potential) after the same depolarizing step. The rate of decay of the tail currents was strongly dependent on membrane potential, with the currents decaying much more rapidly as the membrane potential became more negative. Two-exponential functions (Fig. 3) were fitted to the tail currents to determine the time constants of deactivation of I_{Kr} as a function of membrane potential (Fig. 3B). There was an 8- to 10-fold difference in the magnitude of the “fast” and “slow” time constants and an ~ 2 -fold change in the magnitude of both time constants over the range of membrane potentials from -35 to -65 mV. The membrane potential dependence of the amplitudes of the fast and slow components is shown in Fig. 3C. The components had approximately equal amplitudes at -35 and -45 mV, but for -55 and -65 mV, the fast component was about twice as large as the slow component.

The membrane potential dependence of the activation time constant of I_{Kr} is shown in Fig. 3B. A single-exponential function was adequate to describe the time course of onset of I_{Kr} . The time constant of activation of the current at -30 mV was comparable to the slow time constant of deactivation of the current at -35 mV.

Role of I_{Kr} in repolarization and diastolic depolarization, or pacemaker potential, in adult mouse SAN cells. Figure 4A illustrates the effects of 50 and 200 nM E-4031 on spontaneous

activity from one pacemaker cell recorded with an amphotericin-perforated patch at 35°C . In this cell, E-4031 produced a dose-dependent reduction in maximum diastolic potential, an increase in beat-to-beat interval, and an increase in action potential duration (measured as the 50% repolarization time; Fig. 4A). Compared with control values, the beat-to-beat interval and 50% repolarization time in the presence of E-4031 were very variable. In Fig. 4B, 2-s segments of action potentials from the same cell in control conditions and in the presence of 50 nM and 0.2 μM E-4031 are shown. The E-4031 dose-dependent increase in beat-to-beat interval and the increase in action potential duration resulting from prolongation of repolarization are clearly evident. The higher concentration of E-4031 also produced occasional low-amplitude action potentials with very low rates of rise. Voltage-clamp currents recorded from the same cell before and after application of 0.2 μM E-4031 are also shown in Fig. 4Bc (*inset*). This concentration of E-4031 reduced the net outward current during the -10 -mV depolarizing step and the I_{Kr} tail current at -45 mV by $\sim 60\%$. The effect of E-4031 on spontaneous activity was variable from cell to cell. For example, in three of four cells exposed to 0.2 μM E-4031, the 50% repolarization time and beat-to-beat interval increased from 38.2 ± 2.9 ms and 0.159 ± 0.004 s in control conditions to 55.6 ± 11.0 ms and

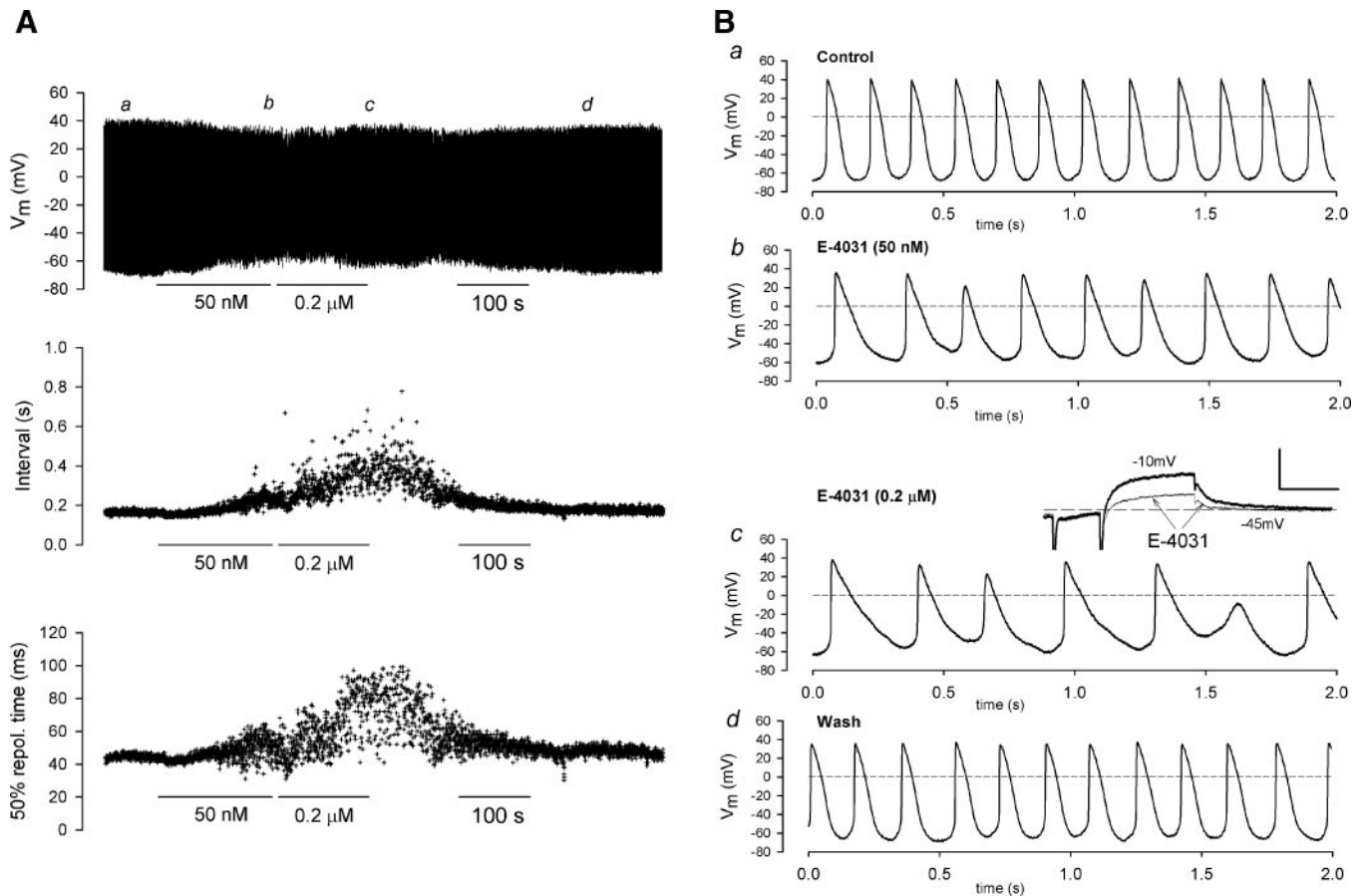


Fig. 4. Effect of E-4031 on spontaneous activity of an isolated sinoatrial node (SAN) cell. **A**: continuous recording of action potentials (*top*), plot of beat-to-beat interval (*middle*), and plot of 50% action potential repolarization (repol) time (*bottom*) before and during exposure to E-4031 and after washout of drug. Amphotericin-perforated-patch recording at $35 \pm 1^\circ\text{C}$ is shown. Cell was exposed to 50 nM and 0.2 μM E-4031. Letters above membrane potential record (*a–d*) identify 2-s intervals plotted in **B**: 2-s segments of control activity (*a*) and activity in 50 nM E-4031 (*b*) and 0.2 μM E-4031 (*c*) and after a 5-min washout of the drug (*d*). *Inset*: voltage-clamp currents recorded from the cell in control conditions and in the presence of E-4031. Current calibration is 100 pA; time calibration is 250 ms.

0.241 ± 0.05 s, respectively, while spontaneous activity in the remaining cell was abolished by 0.2 μM E-4031, and the membrane potential in this cell slowly oscillated between about -20 and -30 mV in the presence of drug. In three different cells, 0.1–1 μM E-4031 abolished spontaneous activity.

Contribution of I_{Kr} to spontaneous action potentials in mouse pacemaker SAN cells. Figure 5, **A** and **B**, compares spontaneous action potentials and the corresponding first derivative of the action potential (dV/dt) waveform recorded from a cell before and after application of 0.2 μM E-4031. Similar to the records shown in Fig. 4, E-4031 produced a decrease in pacing rate, a prolongation of the action potential, and a slight decrease in the maximum diastolic potential. E-4031 also produced significant changes in the waveform of dV/dt during action potential repolarization. In control conditions (Fig. 5A), there was a sharp negative-going “notch” in the dV/dt waveform, with the minimum value of dV/dt (~ -3 V/s) at a membrane potential near -20 mV. This notch was abolished in the presence of 0.2 μM E-4031 (Fig. 5B), and the minimum value of dV/dt was reduced by $\sim 60\%$, with the minimum at a membrane potential close to $+10$ mV.

Changes in I_{Kr} during spontaneous action potentials and the pacemaker depolarization were estimated by applying a volt-

age-clamp protocol that approximated conditions of an “action potential voltage-clamp” method (8) in which the action potential waveform of a SAN cell was simulated by two voltage “ramps.” The membrane potential range, frequency, and ramp durations were chosen to approximate the average properties of spontaneous action potentials recorded in a previous study of pacing SAN cells at 27°C (21). The magnitude and time course of I_{Kr} activated during this simulated “action potential” waveform were determined by subtracting the voltage-clamp currents during application of E-4031 from those before application of the drug. Figure 5C shows membrane currents recorded from one cell before application of E-4031 and the corresponding E-4031-sensitive current. In control conditions, outward current reached a peak ~ 8 ms after the “upstroke” of the action potential waveform. In contrast, the E-4031-sensitive difference current, I_{Kr} , did not reach its peak magnitude until about the midpoint of the repolarization phase of the waveform, ~ 50 ms after the upstroke of the action potential. The peak magnitude of I_{Kr} was $\sim 25\%$ of that of the current before application of E-4031 (Fig. 5C). I_{Kr} declined in amplitude during the later part of repolarization and continued to decline slowly during the diastolic interval of the action potential. Figure 5D is an $I-V$ plot of the mean E-4031-sensitive current recorded from six

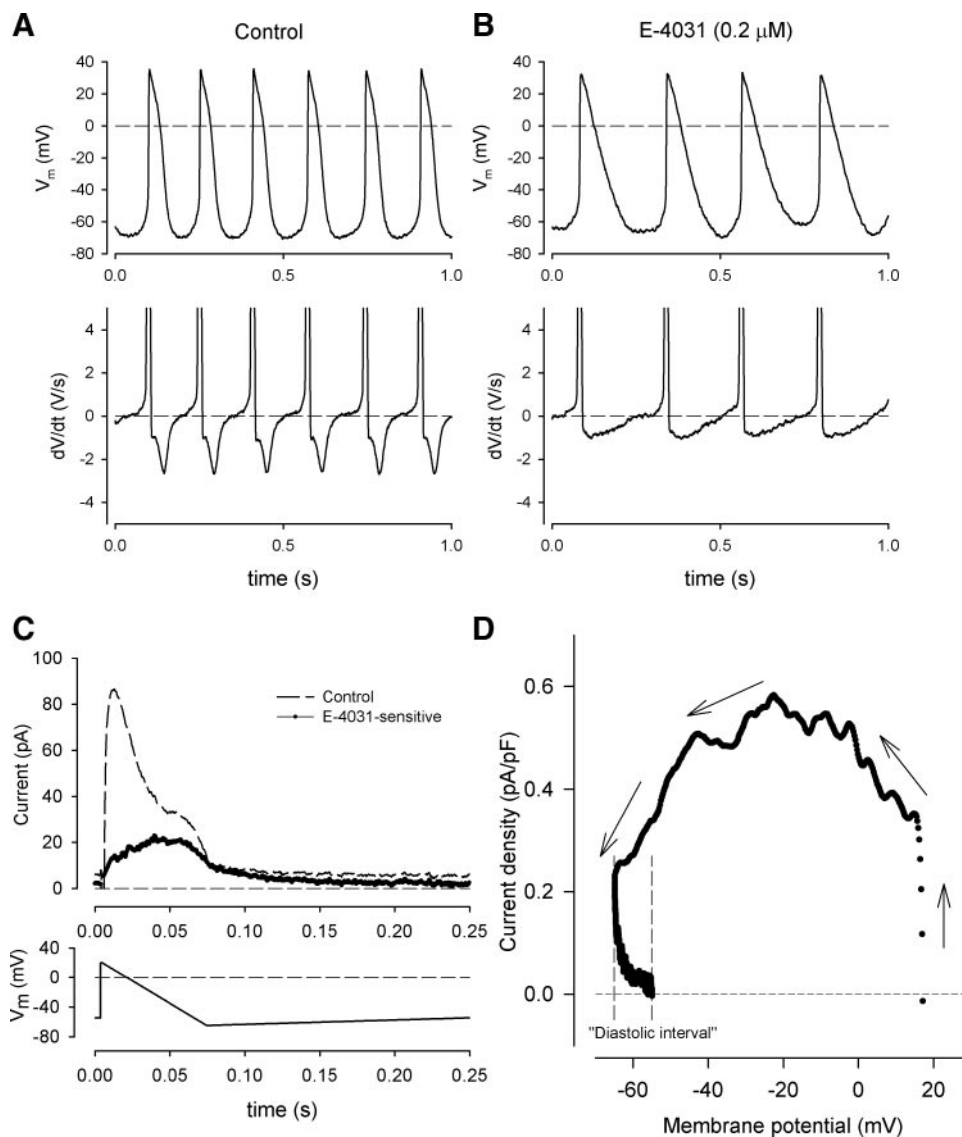


Fig. 5. *A*: spontaneous action potentials (*top*) and 1st derivative of action potential (dV/dt , *bottom*) recorded in control conditions from a cell at $35 \pm 1^\circ\text{C}$. *B*: cell in *A* after application of $0.2 \mu\text{M}$ E-4031. *C*: membrane currents (*top*) from a cell voltage clamped with a simulated SAN "action potential" waveform (*bottom*). Currents from 20 consecutive cycles of the action potential were averaged before and after application of $2.5 \mu\text{M}$ E-4031. E-4031-sensitive difference current was obtained by subtraction. Temperature was $28 \pm 1^\circ\text{C}$. *D*: I - V plot of mean E-4031-sensitive current from 6 different cells voltage clamped with the action potential waveform. Currents from each cell were normalized to capacitance before averaging; mean capacitance of the 6 cells was 25.7 ± 1.1 (SE) pF. Arrows show direction of current trajectory. "Diastolic interval" of simulated action potential is indicated by dashed vertical lines at -65 and -55 mV.

different cells. I_{Kr} reached its maximum magnitude near -25 mV during the repolarization phase of the action potential and declined to nearly zero by the end of the diastolic interval. At the maximum diastolic potential of the waveform, at -65 mV, the mean magnitude of I_{Kr} was ~ 0.25 pA/pF.

Effect of E-4031 on spontaneous sinoatrial rate of Langendorff-perfused mouse hearts. Figure 6 illustrates the effect of E-4031 on the spontaneous sinus rate of Langendorff-perfused mouse hearts. A sample of ECG recordings from one heart that was exposed to $5 \mu\text{M}$ E-4031 is shown in Fig. 6A. The interbeat intervals were significantly prolonged in the presence of E-4031 compared with control values. The effect of E-4031 was reversed in this heart after prolonged (20 min) washout of the drug. Figure 6B summarizes the results of experiments in which five hearts were exposed to $1 \mu\text{M}$ E-4031 and seven different hearts were exposed to $5 \mu\text{M}$ E-4031. Each heart was perfused with control solution for 15 min to ensure that the baseline interval was stable, and the interbeat interval was measured for each heart at 5, 10, and 15 min after the beginning of the perfusion. The control intervals were constant over this time period. The hearts were then exposed to 1 or $5 \mu\text{M}$

E-4031, and interbeat intervals were measured after 5 and 10 min of exposure to the drug. Finally, the drug was removed and intervals were measured 10 and 20 min later. E-4031 at 1 and $5 \mu\text{M}$ produced large increases in the interbeat interval, especially after 10 min of exposure to the drug. The effect of the drug varied considerably from heart to heart. For example, for five different hearts exposed to $1 \mu\text{M}$ E-4031 for 10 min, the increase in interbeat interval ranged from 31.5% to 212% [$74.9 \pm 34.6\%$ (SE)]. There was a similar variability in the effect of $5 \mu\text{M}$ E-4031. The effect of E-4031 on interbeat interval was, on average, only partially reversible, even after 20 min of washout.

Expression of mERG isoforms in the mouse SAN. Expression of mERG genes was compared in the mouse SAN and in the working myocardium (Fig. 7). Expression of mERG1 gene was readily detected by RT-PCR analysis in tissue samples from the SAN, the right atrium, and the left ventricle (Fig. 7B). No detectable bands were found in the absence of reverse transcriptase (Fig. 7B). We studied the expression of three different isoforms of mERG1 (17, 20) (Fig. 7A): mERG1a, mERG1a', and mERG1b. Expression of all these isoforms was consis-

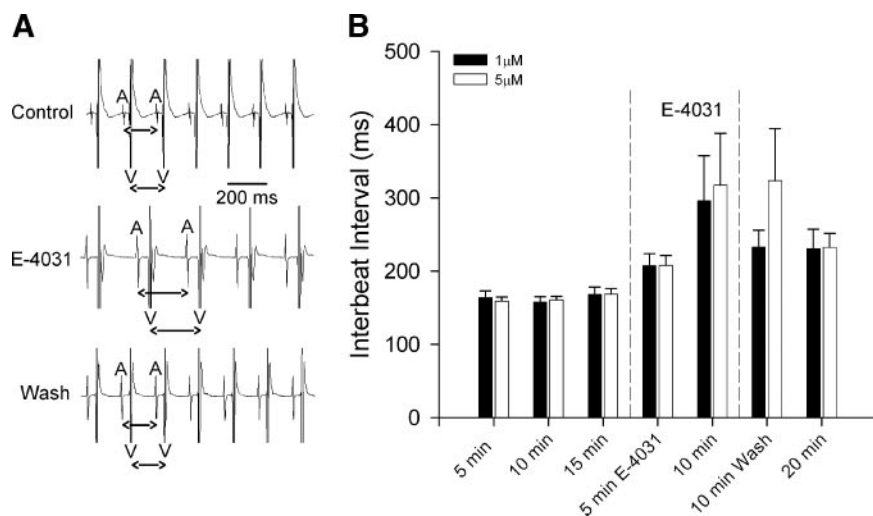


Fig. 6. Effect of E-4031 on sinus rate of Langendorff-perfused mouse heart. A: ECG recordings from a Langendorff-perfused heart. Control was recorded after 15 min in control Krebs-Henseleit solution, E-4031 was recorded after 10 min of exposure to 5 μM E-4031, and wash was recorded 20 min after removal of drug. A and V, ECG deflections associated with atrial and ventricular excitations, respectively. B: plot of interbeat (A-A) interval before, during, and after perfusion with 1 or 5 μM E-4031. Values are means ± SE of 5 hearts for 1 μM E-4031 and 7 different hearts for 5 μM E-4031.

tently found in the mouse SAN (Fig. 7B). In five independent experiments, three specific fragments corresponding to mERG1a, mERG1a', and mERG1b were amplified in tissue samples from the SAN. Expression of mERG1a, mERG1a', and mERG1b was also detected in the right atrium and the left ventricle. The pattern of gene expression was the same in all five experiments. No detectable expression of the other two mERG genes, mERG2 and mERG3, was found in the mouse SAN (data not shown).

DISCUSSION

Biophysical properties of I_{Kr} in adult mouse SAN cells: comparison with other mammalian species. Our results show that I_{Kr} is highly expressed in adult mouse SAN cells. Previous studies have shown that I_{Kr} was also expressed in mouse fetal (7, 38, 39) and neonatal (23, 24, 39) ventricular myocytes. The voltage dependence of “steady-state” activation of I_{Kr} in adult mouse SAN cells (Fig. 2C) was very similar to that of I_{Kr} in fetal mouse ventricular myocytes (38), where the half-activation potential of I_{Kr} tail currents was about -16 mV, compared with about -24 mV for SAN cells (Fig. 2C). The maximum

current density of the I_{Kr} tail currents was ~70% larger in fetal ventricular myocytes (39) than in SAN cells. The voltage dependence of activation of I_{Kr} in mouse SAN cells was also very similar to that reported in rabbit (12, 30) and guinea pig (22) SAN cells.

Deactivation of I_{Kr} in mouse SAN cells was best described by a two-exponential function (Fig. 3) for the voltage range -35 to -65 mV. Similar, two-component deactivation of I_{Kr} has been described in cardiac myocytes of a number of other mammalian species (34). Compared with other mammalian species, I_{Kr} in mouse SAN cells has a somewhat faster rate of deactivation. For example, I_{Kr} in rabbit SAN cells decayed with time constants of 63 and 428 ms at a membrane potential of -60 mV (24). The two time constants of deactivation at -60 mV for I_{Kr} in mouse SAN cells are estimated from Fig. 3B to be ~58 and 372 ms. Although these values are similar to the time constants for rabbit SAN, the experiments of Ono and Ito (24) were carried out at 35°C, compared with 28°C for the mouse experiments. The mouse I_{Kr} deactivation time constants can be corrected from 28°C to 35°C using a Q_{10} of 1.4, the approximate value of the temperature dependence of the deac-

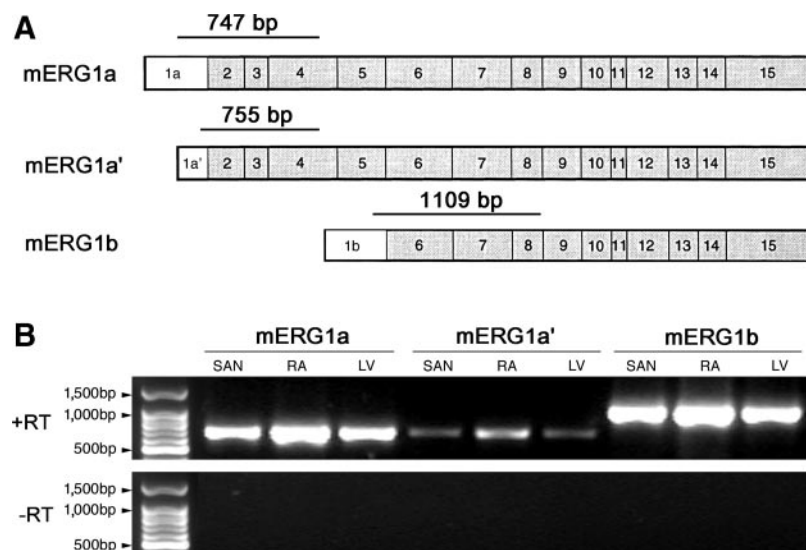


Fig. 7. Cardiac tissue distribution of mERG1 isoforms. A: exon structure of mERG1 transcripts. Relative positions of amplified fragments, together with their predicted sizes, are indicated above each isoform. B: RT-PCR products derived from SAN, right atrium (RA), and left ventricle (LV) using oligonucleotide sets that specifically recognized the reverse-transcribed mRNA encoding mERG1a, mERG1a', and mERG1b (see METHODS).

tivation rate of HERG K^+ channels heterologously expressed in HEK 293 cells (42). The HERG gene and its homologs are thought to encode I_{Kr} channels in mammalian cardiac cells (27). With the use of a Q_{10} correction of 1.4, the time constants of deactivation of mouse SAN I_{Kr} at -60 mV are estimated to be ~ 36 and 230 ms at 35°C , substantially less than the corresponding time constants for rabbit SAN. In addition, there is a significant difference between mouse and rabbit SAN in the relative contribution of the amplitudes of the fast and slow components to the time course of decay of I_{Kr} . In rabbit, the fast component comprised 50–60% of the initial amplitude of I_{Kr} tail currents, and this ratio was not significantly dependent on membrane potential. In mouse, the fast component of the I_{Kr} tail current amplitude varied from $\sim 50\%$ at -35 mV to $\sim 74\%$ at -65 mV (Fig. 3B). On the basis of these differences in the relative amplitudes of the fast and slow components and their respective time constants, I_{Kr} tail current in mouse SAN cells would decay to one-half of its initial amplitude in ~ 37 ms, $\sim 40\%$ of the time required for rabbit SAN I_{Kr} to decay to the same level at -60 mV. The relatively rapid deactivation of mouse I_{Kr} compared with I_{Kr} in rabbit and guinea pig SAN may contribute to the higher heart rate of mouse.

Role of I_{Kr} in action potential repolarization and pacemaking in mouse SAN cells. The data in Figs. 4 and 5 clearly show that I_{Kr} is very important in controlling action potential repolarization and pacemaking in mouse SAN cells. Even partial block of I_{Kr} by E-4031 (Fig. 4B) resulted in substantial prolongation of final repolarization of action potentials and a slowing in spontaneous rate, and in some cells spontaneous activity was completely arrested. Similar effects of E-4031 on action potential repolarization and spontaneous activity have been reported in rabbit (14, 24, 35) and guinea pig (22) SAN cells. In rabbit SAN cells, the effect of E-4031 was dependent on the region of the node from which action potentials were recorded (14). At a concentration of E-4031 that only partially blocked I_{Kr} ($0.1 \mu\text{M}$), spontaneous activity recorded from cells in the central part of the SAN was completely abolished, whereas spontaneous activity recorded from cells in peripheral parts of the node was not abolished, but the rate of activity was reduced, action potential repolarization was slowed, and maximum diastolic potential was reduced. These differences in the effects of E-4031 on spontaneous activity in central and peripheral regions of the rabbit SAN may be related in part to a heterogeneous expression of I_{Kr} (19). Possibly, the variability in response of mouse SAN cells to I_{Kr} block by E-4031 results from a similar heterogeneous expression of I_{Kr} throughout the SAN. Alternatively, depolarization of the maximum diastolic potential and prolongation of the action potential duration will translate into less activation of hyperpolarization-activated current and availability of L-type Ca^{2+} channel current during the diastolic depolarization and upstroke phase of the action potential. Thus the net effect of E-4031 on pacemaking will reflect I_{Kr} block by the drug and altered recruitment of other ionic currents.

Action potential voltage clamp (8) has been used to determine the magnitude and time course of I_{Kr} during spontaneous activity in SAN (24, 41) cells of rabbit. In rabbit SAN cells (24), the peak systolic magnitude of I_{Kr} (E-4031-sensitive current) was 2–3 pA/pF, with maximum current at -46 mV. The current declined during late repolarization but remained outward and approximately constant during the entire diastolic

interval, with a density of 0.4–0.6 pA/pF (24). In mouse SAN cells, I_{Kr} declined nearly to zero by the end of the diastolic interval. The maximum outward I_{Kr} in mouse SAN cells occurred at approximately -25 mV and was smaller (~ 0.6 pA/pF; Fig. 5D) than the maximum systolic current in rabbit SAN cells (1.6 pA/pF, at -20 mV). The current density at the “maximum diastolic potential” of the simulated action potential, 0.26 pA/pF, was only about one-half of that in rabbit SAN cells. Direct comparison of the magnitude and time course of I_{Kr} in mouse and rabbit pacemaking cells is difficult because of different experimental conditions; the experiments with rabbit cells were done at 35 – 37°C , compared with 28°C for mouse cells. Also, recorded spontaneous action potentials were used as the voltage-clamp “command” potential for rabbit cells, whereas a simulated action potential (with parameters typical of spontaneous action potentials at 27°C) was used in the mouse studies. However, despite differences in experimental conditions, the qualitative agreement between I_{Kr} recorded from rabbit and mouse pacemaker cells in these action potential voltage-clamp experiments suggests that I_{Kr} has a very similar role in regulating action potential repolarization and pacemaker activity in the mouse and larger mammals.

Spontaneous pacemaker activity (Figs. 4 and 5) of mouse SAN cells was recorded using amphotericin-perforated patches at 35°C in the presence of 10 nM Iso. It has previously been shown in guinea pig ventricular myocytes that I_{Kr} tail current amplitudes were increased by $\sim 50\%$ by 10 – 100 nM Iso when recordings were made with amphotericin-perforated patches (10). It is possible, therefore, that β -adrenergic stimulation by Iso increased the magnitude of I_{Kr} during an action potential compared with basal conditions. The net effect of such an increase in I_{Kr} on action potential waveform and frequency of spontaneous activity is complicated by the concomitant increase in other currents that importantly contribute to pacemaker activity, such as hyperpolarization-activated and L-type Ca^{2+} channel currents, which are also stimulated by β -agonists.

Effect of blocking I_{Kr} on isolated heart preparations and in vivo. At 1 – $5 \mu\text{M}$, E-4031 had much less effect on the spontaneous sinoatrial rate of Langendorff-perfused hearts than on the spontaneous rate of isolated SAN cells. Such concentrations of E-4031 invariably arrested the spontaneous activity of single cells. E-4031 ($0.1 \mu\text{M}$) produced an $\sim 18\%$ decrease in heart rate of Langendorff-perfused adult rat hearts (31), whereas in isolated fetal rat hearts, dofetilide ($1 \mu\text{M}$) produced a $>50\%$ decrease in heart rate (1). These changes in heart rate are in the same range as those recorded in isolated Langendorff-perfused mouse hearts (Fig. 6). Reasons for the differences in the sensitivity of spontaneous activity of isolated hearts and single cells in response to the block of I_{Kr} by E-4031 are unclear. In intact sinoatrial preparations of rabbit heart (14), $1 \mu\text{M}$ E-4031 decreased sinoatrial rate from 103 beats/min (32°C) to 79 beats/min, and the leading or primary pacemaker site shifted from the central region of the node to a more peripheral region nearer the superior vena cava and the crista terminalis. Cells in peripheral regions of the rabbit SAN have a higher density of I_{Kr} than central nodal cells (19); hence, blocking a fraction of I_{Kr} may have less effect on spontaneous activity in the peripheral cells than in the central cells. It is possible that the variability in response of mouse SAN cells to E-4031 resulted from a similar nonhomogeneous expression of

I_{Kr} throughout the mouse SAN. Microelectrode recordings of action potentials in different regions of intact SAN of mouse have made a clear distinction between central "primary" and more peripheral "secondary" pacemaker cells (36). It is possible that shifts in primary pacemaker location also occur in the intact mouse SAN in the presence of E-4031, allowing spontaneous activity to continue, even when a substantial fraction of I_{Kr} is blocked. An alternative explanation for the relatively small effect of I_{Kr} block on the pacemaker activity of the intact heart compared with isolated pacemaker cells is suggested by the recent work of Verheijck and colleagues (37). They showed that when the rabbit SAN was separated from the atrium, block of I_{Kr} by E-4031 resulted in pacemaker arrest in the SAN. However, when the SAN was not separated from the atrium, spontaneous activity was not halted, even though action potential configurations in the SAN were profoundly altered, e.g., reduced amplitude and maximum diastolic potential, and slowed final repolarization. This effect of the intact atrium was attributed to a hyperpolarizing influence exerted by the atrium on the SAN, which allowed pacemaking to continue, even in the absence of a major SAN pacemaker current.

Expression of mERG1. Previous evidence has suggested that native cardiac I_{Kr} is composed of mERG1a in association with different splice variants and/or accessory subunits, such as proteins coded by the KCNE gene family (25). In this study, we found evidence of the expression of three different isoforms of mERG1 at the mRNA level: the full-length mERG1a transcript and the two variants mERG1a' and mERG1b with shorter NH₂ terminus. In our study, it was not possible on the basis of mERG1 expression pattern alone to determine which mERG1 isoforms are expressed at the protein level and contribute to the ion channels that underlie the native I_{Kr} in the mouse SAN. However, heterologous coexpression of mERG1a and mERG1b produced currents with kinetic properties that were more similar to that of native I_{Kr} than currents obtained by expressing the two isoforms individually (20), and the cardiac-specific mERG1b has been reported to produce I_{Kr} similar to that recorded in cardiac myocytes (17). Also, consistent with our RT-PCR results, selective inactivation of mERG1b in the mouse strongly reduced I_{Kr} in fetal myocytes (16) and induced episodes of sinoatrial bradycardia, thus indicating a specific contribution of this isoform to in vivo pacemaking and formation of the native mouse SAN I_{Kr}. We cannot completely rule out that other unknown isoforms of mERG1 are expressed in the mouse SAN, but because we did not find evidence for the expression of known genes other than mERG1, our results further support the view that the mERG1 gene constitutes the molecular basis of native mouse SAN I_{Kr}.

Summary. This study shows that I_{Kr} is robustly expressed in SAN pacemaker cells in adult mouse heart and plays an essential role in regulating action potential duration and pacemaker activity in the mouse SAN. Biophysical properties of I_{Kr} in adult mouse SAN, such as its magnitude, voltage dependence of activation, and inward rectification, are similar to those of I_{Kr} in other mammalian SAN, e.g., guinea pig and rabbit, but deactivation of mouse I_{Kr} in the range of diastolic membrane potentials is faster than that of larger mammals. This is consistent with the role of I_{Kr} as a pacemaker current in a heart with the very high spontaneous heart rate (~500–600 beats/min) of the mouse. Further clarification of the role of I_{Kr} in regulating spontaneous activity in adult mouse SAN will

require detailed examination of the phenotype of genetically engineered mice in which mERG1 isoforms have been selectively inactivated.

ACKNOWLEDGMENTS

Present address of W. R. Giles: Dept. of Bioengineering, University of California San Diego, La Jolla, CA 92093-0412.

GRANTS

This work was supported by operating grants from the Canadian Institutes of Health Research and the Heart and Stroke Foundation of Canada (to W. R. Giles) and the Association Française Contre les Myopathies and the Action Concertée Incitative in Developmental Biology of the French Ministry for Education (to J. Nargeot). M. E. Mangoni acknowledges a postdoctoral fellowship from the Lefoulon-Delalande Foundation. W. R. Giles holds a Research Chair sponsored by the Heart and Stroke Foundation of Alberta.

REFERENCES

1. Abrahamsson C, Palmer M, Ljung B, Duker G, Bäärnhielm C, Carlsson L, and Danielsson B. Induction of rhythm abnormalities in the fetal rat heart. A tentative mechanism for the embryotoxic effect of the class III antiarrhythmic agent almokalant. *Cardiovasc Res* 28: 337–344, 1994.
2. Apkon M and Nerbonne JM. Characterization of two distinct depolarization-activated K⁺ currents in isolated adult rat ventricular myocytes. *J Gen Physiol* 97: 973–1011, 1991.
3. Babji P, Askew GR, Nieuwenhuijsen B, Su CM, Bridal TR, Jow B, Argentero TM, Kulik J, DeGennaro LJ, Spinelli W, and Colatsky TJ. Inhibition of cardiac delayed rectifier K⁺ current by overexpression of the long-QT syndrome HERG G628S mutation in transgenic mice. *Circ Res* 83: 668–678, 1998.
4. Boyett MR, Honjo H, and Kodama I. The sinoatrial node, a heterogeneous pacemaker structure. *Cardiovasc Res* 47: 658–687, 2000.
5. Boyle WA and Nerbonne JM. Two functionally distinct 4-aminopyridine-sensitive outward K⁺ currents in rat atrial myocytes. *J Gen Physiol* 100: 1041–1067, 1992.
6. Cho HS, Takano M, and Noma A. The electrophysiological properties of spontaneously beating pacemaker cells isolated from mouse sinoatrial node. *J Physiol* 550: 169–180, 2003.
7. Davies MP, An RH, Doevendans P, Kubalak S, Chien KR, and Kass RS. Developmental changes in ionic channel activity in the embryonic murine heart. *Circ Res* 78: 15–25, 1996.
8. Doerr T, Denger R, and Trautwein W. Calcium currents in single SA nodal cells of the rabbit heart studied with action potential clamp. *Pflügers Arch* 413: 599–603, 1989.
9. Hamill OP, Marty A, Neher E, Sakmann B, and Sigworth FJ. Improved patch-clamp techniques for high-resolution current recording from cells and cell-free membrane patches. *Pflügers Arch* 391: 85–100, 1981.
10. Health BM and Terrar DA. Protein kinase C enhances the rapidly activating delayed rectifier potassium current, I_{Kr}, through a reduction in C-type inactivation in guinea-pig ventricular myocytes. *J Physiol* 522: 391–402, 2000.
11. Irisawa H, Brown HF, and Giles W. Cardiac pacemaking in the sinoatrial node. *Physiol Rev* 73: 197–227, 1993.
12. Ito H and Ono K. A rapidly activating delayed rectifier K⁺ channel in rabbit sinoatrial node cells. *Am J Physiol Heart Circ Physiol* 269: H443–H452, 1995.
13. Keating M and Sanguinetti MC. Molecular and cellular mechanisms of cardiac arrhythmias. *Cell* 104: 569–580, 2001.
14. Kodama I, Boyett MR, Nikmaram MR, Yamamoto M, Hojo H, and Niwa H. Regional differences in effects of E-4031 within the sinoatrial node. *Am J Physiol Heart Circ Physiol* 276: H793–H802, 1999.
15. Kupersmidt S, Yang T, Anderson ME, Wessels A, Niswender KD, Magnuson MA, and Roden DM. Replacement by homologous recombination of the minK gene with lacZ reveals restriction of minK expression to the mouse cardiac conduction system. *Circ Res* 84: 146–152, 1999.
16. Lees-Miller JP, Guo G, Somers JR, Roach RS, Sheldon RS, Rancourt DE, and Duff HJ. Selective knockout of mouse ERG1B potassium channel eliminates I_{Kr} in adult ventricular myocytes and elicits episodes of abrupt sinus bradycardia. *Mol Cell Biol* 23: 1856–1862, 2003.
17. Lees-Miller JP, Kondo C, Wang L, and Duff HJ. Electrophysiological characterization of an alternatively processed ERG K⁺ channel in mouse and human hearts. *Circ Res* 81: 719–726, 1997.

18. **Lei M and Brown HF.** Two components of the delayed rectifier potassium current, I_K , in rabbit sino-atrial node cells. *Exp Physiol* 81: 725–741, 1996.
19. **Lei M, Honjo H, Kodama I, and Boyett MR.** Heterogeneous expression of the delayed-rectifier K^+ currents $i_{K,r}$ and $i_{K,s}$ in rabbit sinoatrial node cells. *J Physiol* 535: 703–714, 2001.
20. **London B, Trudeau MC, Newton KP, Beyer AK, Copeland NG, Gilbert DJ, Jenkins NA, Satler CA, and Robertson GA.** Two isoforms of the mouse ether-a-go-go-related gene coassemble to form channels with properties similar to the rapidly activating component of the cardiac delayed rectifier K^+ current. *Circ Res* 81: 870–878, 1997.
21. **Mangoni ME and Nargeot J.** Properties of the hyperpolarization-activated current (I_f) in isolated mouse sino-atrial cells. *Cardiovasc Res* 52: 51–64, 2001.
22. **Matsuura H, Ehara T, Ding WG, Omatsu-Kanbe M, and Isono T.** Rapidly and slowly activating components of delayed rectifier K^+ current in guinea-pig sino-atrial node pacemaker cells. *J Physiol* 540: 815–830, 2002.
23. **Nuss HB and Marban E.** Electrophysiological properties of neonatal mouse cardiac myocytes in primary culture. *J Physiol* 479: 265–279, 1994.
24. **Ono K and Ito H.** Role of rapidly activating delayed rectifier K^+ current in sinoatrial node pacemaker activity. *Am J Physiol Heart Circ Physiol* 269: H453–H462, 1995.
25. **Pond AL, Scheve BK, Benedict AT, Petrecca K, Van Wagoner DR, Shrier A, and Nerbonne JM.** Expression of distinct ERG proteins in rat, mouse and human heart. Relation to functional I_{Kr} channels. *J Biol Chem* 275: 5997–6006, 2000.
26. **Rae J, Cooper K, Gates P, and Watsky M.** Low access resistance perforated patch recordings using amphotericin B. *J Neurosci Methods* 37: 15–26, 1991.
27. **Sanguinetti MC, Jiang C, Curran ME, and Keating MT.** A mechanistic link between an inherited and an acquired cardiac arrhythmia: HERG encodes the I_{Kr} potassium channel. *Cell* 81: 299–307, 1995.
28. **Sanguinetti MC and Jurkiewicz NK.** Two components of cardiac delayed rectifier K^+ current. Differential sensitivity to block by class III antiarrhythmic agents. *J Gen Physiol* 96: 195–215, 1990.
29. **Sanguinetti MC and Jurkiewicz NK.** Delayed rectifier outward K^+ current is composed of two currents in guinea pig atrial cells. *Am J Physiol Heart Circ Physiol* 260: H393–H399, 1991.
30. **Shibasaki T.** Conductance and kinetics of delayed rectifier potassium channels in nodal cells of the rabbit heart. *J Physiol* 387: 227–250, 1987.
31. **Shinmura K, Tani M, Hasegawa H, Ebihara Y, and Nakamura Y.** Effect of E-4031, a class III antiarrhythmic drug, on ischemia- and reperfusion-induced arrhythmias in isolated rat hearts. *Jpn Heart J* 39: 183–197, 1998.
32. **Spector PS, Curran ME, Zou A, Keating MT, and Sanguinetti MC.** Fast inactivation causes rectification of the I_{Kr} channel. *J Gen Physiol* 107: 611–619, 1996.
33. **Tande PM, Bjornstad H, Yang T, and Refsum H.** Rate-dependent class III antiarrhythmic action, negative chronotropy and positive inotropy of a novel I_K blocking drug, UK-68798: potent in guinea-pig but no effect in rat myocardium. *J Cardiovasc Pharmacol* 16: 401–410, 1990.
34. **Tseng GN.** I_{Kr} : the hERG channel. *J Mol Cell Cardiol* 33: 835–849, 2001.
35. **Verheijck EE, van Ginneken AC, Bourier J, and Bouman LN.** Effects of delayed rectifier current blockade by E-4031 on impulse generation in single sinoatrial nodal myocytes of the rabbit. *Circ Res* 76: 607–615, 1995.
36. **Verheijck EE, van Kempen MJA, Veereschild M, Lurvink J, Jongasma HJ, and Bouman LN.** Electrophysiological features of the mouse sino-atrial node in relation to connexin distribution. *Cardiovasc Res* 52: 40–50, 2001.
37. **Verheijck EE, Wilders R, and Bouman LN.** Atrio-sinus interaction demonstrated by blockade of the rapid delayed rectifier current. *Circulation* 105: 880–885, 2002.
38. **Wang L and Duff HJ.** Identification and characteristics of delayed rectifier K^+ current in fetal mouse ventricular myocytes. *Am J Physiol Heart Circ Physiol* 270: H2088–H2093, 1996.
39. **Wang L, Feng ZP, Kondo CS, Sheldon RS, and Duff HJ.** Developmental changes in the delayed rectifier K^+ channels in mouse heart. *Circ Res* 79: 79–85, 1996.
40. **Wymore RS, Gintant GA, Wymore RT, Dixon JE, McKinnon D, and Cohen IS.** Tissue and species distribution of mRNA for the I_{Kr} -like K^+ channel, erg. *Circ Res* 80: 261–268, 1997.
41. **Zaza A, Micheletti M, Brioschi A, and Rocchetti M.** Ionic currents during sustained pacemaker activity in rabbit sino-atrial myocytes. *J Physiol* 505: 677–688, 1997.
42. **Zhou Z, Gong Q, Ye B, Fan Z, Makielski JC, Robertson GA, and January CT.** Properties of HERG channels stably expressed in HEK 293 cells studied at physiological temperature. *Biophys J* 74: 230–241, 1998.